PHYSICAL REVIEW E **88**, 020302(R) (2013)

Holographic measurements of anisotropic three-dimensional diffusion of colloidal clusters

Jerome Fung
Department of Physics, Harvard University, Cambridge, Massachusetts 02138, USA

Vinothan N. Manoharan*
School of Engineering and Applied Sciences, Harvard University, Cambridge, Massachusetts 02138, USA
and Department of Physics, Harvard University, Cambridge, Massachusetts 02138, USA
(Received 6 May 2013; published 30 August 2013)

We measure all nonzero elements of the three-dimensional diffusion tensor **D** for clusters of colloidal spheres to a precision of 1% or better using digital holographic microscopy. We study both dimers and triangular trimers of spheres, for which no analytical calculations of the diffusion tensor exist. We observe anisotropic rotational and translational diffusion arising from the asymmetries of the clusters. In the case of the three-particle triangular cluster, we also detect a small but statistically significant difference in the rotational diffusion about the two in-plane axes. We attribute this difference to weak breaking of threefold rotational symmetry due to a small amount of particle polydispersity. Our experimental measurements agree well with numerical calculations and show how diffusion constants can be measured under conditions relevant to colloidal self-assembly, where theoretical and even numerical prediction is difficult.

DOI: 10.1103/PhysRevE.88.020302 PACS number(s): 82.70.Dd, 36.40.Sx, 42.40.Kw

Diffusion plays a critical role in the dynamics, self-assembly, and rheology of complex fluids. In systems such as colloidal suspensions, which typically have short-ranged interaction potentials, diffusion can in fact play a larger role than energy barriers in setting transition rates [1]. However, the diffusion of geometrically anisotropic particles, a common class of colloidal suspension that can also arise as intermediates in the self-assembly of spherical particles, can be difficult to predict. Theoretically determining friction factors for these particles requires analytically solving Stokes's equation, which is only possible for highly symmetric particles such as ellipsoids [2] or sphere dimers [3] in unbounded fluids. Numerical methods such as bead modeling [4] or finite-element methods [5–7] require approximating the shape of the particles or the hydrodynamic interactions. These methods are difficult to apply when asymmetric particles diffuse near rigid boundaries or other particles, two situations that are relevant to colloidal self-assembly and dynamics in general. Thus experimental measurements of diffusion tensors are crucial.

In particular, precision measurements on single particles rather than ensembles are necessary. Anisotropic particles show multiple diffusion time scales that are difficult to resolve through bulk techniques such as depolarized dynamic light scattering [8]. However, there have been few single-particle studies of anisotropic diffusion in three dimensions. Video microscopy has been used to measure two-dimensional (2D) diffusion of colloidal ellipsoids [9,10] and planar sphere clusters [11], but the technique yields limited information about out-of-plane motions [12–14]. Confocal microscopy can be used to study the three-dimensional (3D) dynamics of geometrically anisotropic particles, but has only been applied to highly symmetric particles [15,16] and is limited by the time (∼1 s) needed to acquire a 3D stack. This can make it challenging to probe time scales comparable to particle diffusion times or to study rare processes such as the early stages of self-assembly [17].

In this Rapid Communication, we study the 3D diffusion of individual colloidal clusters. We measure the diffusion tensor using a fast 3D imaging technique, in-line digital holographic microscopy, which involves recording a 2D hologram generated by interference between light scattered from colloidal particles and the undiffracted transmitted beam [Fig. 1(a)] [18]. Unlike 3D confocal stacks, 2D holograms can be recorded at submillisecond frame rates. By fitting models based on electromagnetic scattering solutions to the holograms [18–20], we recover the 3D dynamics of dimers and triangular trimers of colloidal spheres. We resolve all the translational and rotational components of the diffusion tensor to 1% precision or better. We experimentally demonstrate the effects of asymmetry on diffusion and even show that a small amount of polydispersity results in symmetry breaking in the rotational diffusion tensor components. Our measurements agree well with numerical calculations and, more generally, show how diffusion tensors can be measured in experimental systems relevant to self-assembly, where theoretical predictions are challenging.

The diffusion tensor **D** quantifies the translational and rotational Brownian diffusion of an arbitrary rigid colloidal particle. In general, six generalized coordinates q^i (three positions and three orientation angles) are needed to describe the position and orientation of a rigid body. Although **D** is rigorously defined by generalizing Fick's law to an abstract ensemble of particles diffusing in this six-dimensional configuration space, **D** also describes correlations between displacements of the q^i for short lag times τ [22,23]:[1]

$$\langle \Delta q^i \, \Delta q^j \rangle = 2D^{ij}\tau. \quad (1)$$

*vnm@seas.harvard.edu

[1]Equation (1) strictly applies only for short τ because it assumes small changes in the generalized particle probability density arising from diffusion for short τ [22].

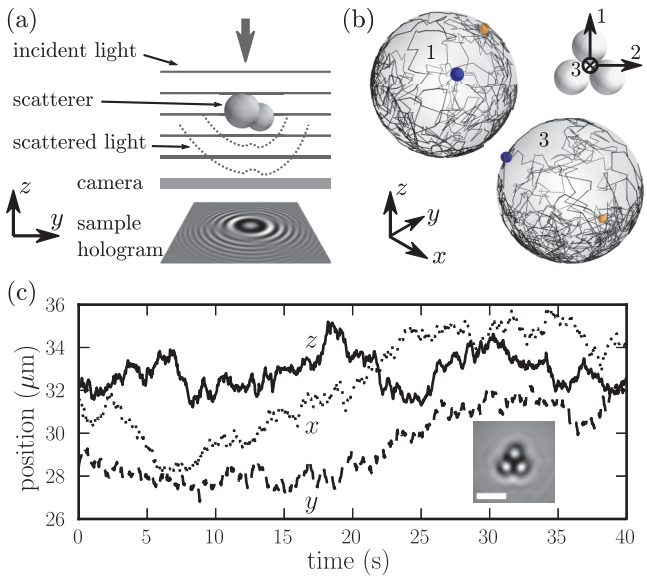

FIG. 1. (Color online) (a) Schematic overview of the in-line holographic microscope used in the experiments. The inset shows the orientation of the laboratory-frame axes. (b) Axis trajectories for a diffusing triangular cluster of 1-μm-diam polystyrene spheres (the inset shows the orientation of the laboratory-frame axes). Renderings show the trajectories of axes 1 and 3 on a unit sphere. Blue (dark) markers indicate the start of the 40-s trajectory and orange (light) markers the end. (c) Laboratory-frame center-of-mass trajectories of the same triangular cluster over the same time interval as in (b). The inset shows the amplitude reconstruction [21] of a recorded trimer hologram, showing the cluster structure. The scale bar is 2 μm.

Further, $\mathbf{D}$ may be partitioned into the following 3×3 blocks:

$$\mathbf{D} = \begin{pmatrix} \mathbf{D}^{tt} & \mathbf{D}^{\dagger tr} \\ \mathbf{D}^{tr} & \mathbf{D}^{rr} \end{pmatrix} \tag{2}$$

Here $\mathbf{D}^{tt}$ describes translational diffusion, $\mathbf{D}^{rr}$ rotational diffusion, and $\mathbf{D}^{tr}$ translation-rotation coupling. The generalized Stokes-Einstein equation relates $\mathbf{D}$ to the friction tensor $\mathfrak{F}$ describing the hydrodynamic Stokes drag forces and torques on a moving particle: $\mathbf{D} = k_B T \mathfrak{F}^{-1}$ [22,23]. Predicting $\mathbf{D}$ thus requires a solution for the Stokes flow around a particle. Dimers are one of the few nonspherical shapes for which analytical solutions exist; none exist for trimers.

We make dimer and triangular trimer clusters through limited aggregation of sulfate polystyrene spheres (Invitrogen) [24], 1.3-μm in diameter for dimers and 1-μm in diameter for trimers. We transfer these particles into a 250-mM NaCl solution to screen the charge of the stabilizing sulfate groups and start the aggregation and then we decrease the ionic strength by quenching with deionized water (Millipore) after 1 min to arrest the aggregation. We then suspend the resulting mixture of single particles, dimers, and larger clusters in a density-matched solvent consisting of 50% v/v D_2O and 50% v/v H_2O with a salt concentration of 1 mM. We load the particles into sample cells made from glass slides, coverslips, and 76-μm-thick Mylar spacers [19,20]. After finding a cluster with the desired morphology using bright field microscopy, we ensure that it is at least 30 μm away from sample cell walls or other particles so that the cluster diffusion is unhindered by boundaries [25]. We record holograms using an instrument previously described in the literature [17,20] at a frame rate of 25 frames/s and at ambient temperature $T = 296^{+2}_{-4}$ K.

We then analyze the measured holograms to obtain 3D trajectories of the clusters. We obtain particle sizes, refractive indices, center-of-mass 3D positions, and three orientation angles (two for dimers) by fitting an exact scattering solution to Maxwell's equations to each recorded hologram [19,26,27]. Figures 1(b) and 1(c) show some of the 3D data we obtain for a trimer. We measure the components of the translational block $\mathbf{D}^{tt}$ by directly applying Eq. (1), where the relevant Δq^i are relative to a coordinate system rigidly fixed to the cluster [19,22,23]. The correlation functions needed to measure the diagonal components of $\mathbf{D}^{tt}$ are cluster-frame mean-squared displacements (MSDs). To measure the components of $\mathbf{D}^{rr}$, we examine the dynamics of the axis vectors $\mathbf{u}_i$ fixed to a cluster. The tips of the $\mathbf{u}_i$ diffuse along the surface of a unit sphere, as illustrated in Fig. 1(b). We compute autocorrelations of the $\mathbf{u}_i$, which are related to $D_{r,i}$, the three diagonal components of $\mathbf{D}^{rr}$, as follows [28]:

$$\langle \mathbf{u}_i(t) \cdot \mathbf{u}_i(t+\tau) \rangle = \exp\left[\left(D_{r,i} - \sum_j D_{r,j} \right) \tau \right] \tag{3}$$

For the axisymmetric dimer, we consider a related quantity, the MSD of the axis unit vector $\mathbf{u}$ [15,19,29,30]:

$$\langle \Delta \mathbf{u}^2(\tau) \rangle = 2[1 - \langle \mathbf{u}(t) \cdot \mathbf{u}(t+\tau) \rangle]. \tag{4}$$

We find good agreement between $\mathbf{D}$ for a dimer, measured to 0.5% precision [27] from a time series of 22 000 holograms, and analytical and numerical predictions. The measured axis MSD, along with a best fit to Eq. (4), and the cluster-frame MSDs are shown in Fig. 2. Dimers of two identical spheres have three mirror planes and an axis of continuous rotational symmetry, so in the coordinate system shown in the inset of Fig. 2(b), $\mathbf{D}$ is diagonal. However, due to the breaking of spherical symmetry, $\mathbf{D}$ has four rather than two unique elements: the translational diffusion constants $D_\parallel$ and $D_\perp$ and the rotational diffusion constants $D_{r,\parallel}$ and $D_{r,\perp}$ [19,22]. The subscripts denote translations along, or rotations about, the dimer symmetry axis ($\parallel$) and the two degenerate perpendicular axes ($\perp$). Because we cannot observe rotations about the dimer axis, we can only measure $D_{r,\perp}$. Moreover, we can only measure a combined MSD $\langle \Delta x_\perp(\tau)^2 \rangle$ along the perpendicular axes. We then extract $D_\parallel$ and $D_\perp$ from linear fits to the MSDs. The MSD $\langle \Delta x_\parallel^2(\tau) \rangle$ has a slope of $2D_\parallel$ in accordance with Eq. (1) and $\langle \Delta x_\perp^2(\tau) \rangle$ has a slope of $4D_\perp$. Our measurement of $D_\parallel / D_\perp$, which is a universal constant for any Brownian dimer, agrees well with predictions from the shell modeling code HYDROSUB [31] and the exact Stokes solution of Nir and Acrivos [3] (Table I).

The individual elements of $\mathbf{D}$ also agree with calculations, once we account for the sphere radius a and the solvent viscosity η. We determine an effective sphere radius a_{eff} from the measured ratios $D_\parallel / D_{r,\perp}$ and $D_\perp / D_{r,\perp}$, which depend only on a [3]. Then we determine the best-fit η_{eff} from the measured elements of $\mathbf{D}$. We find an effective

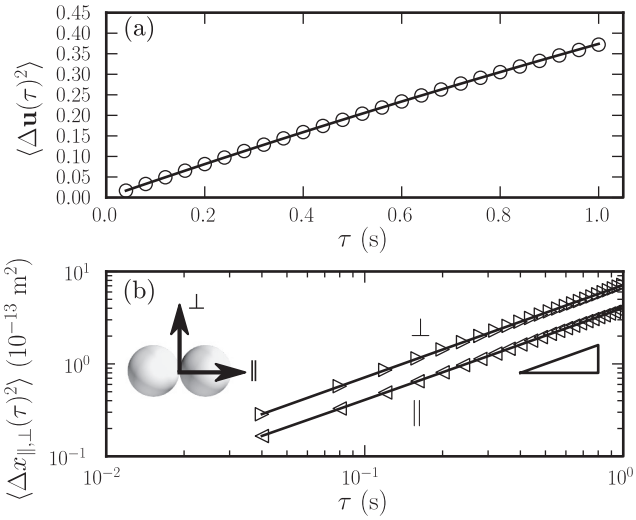

FIG. 2. (a) Axis MSD for dimer of 1.3-μm-diam spheres. Open symbols are measurements; the solid line is the best fit to Eq. (4), where $\langle \mathbf{u}(t) \cdot \mathbf{u}(t+\tau) \rangle = \exp(-2D_{r,\perp}\tau)$. (b) Cluster-frame MSD computed for the same dimer as in (a). Open symbols are measurements; solid lines are linear fits. The triangle shows a slope of 1. Error bars are calculated using a block decorrelation technique [32]; they are comparable in size to the plotting symbols or smaller. The inset shows the orientation of parallel ($\parallel$) and perpendicular ($\perp$) axes.

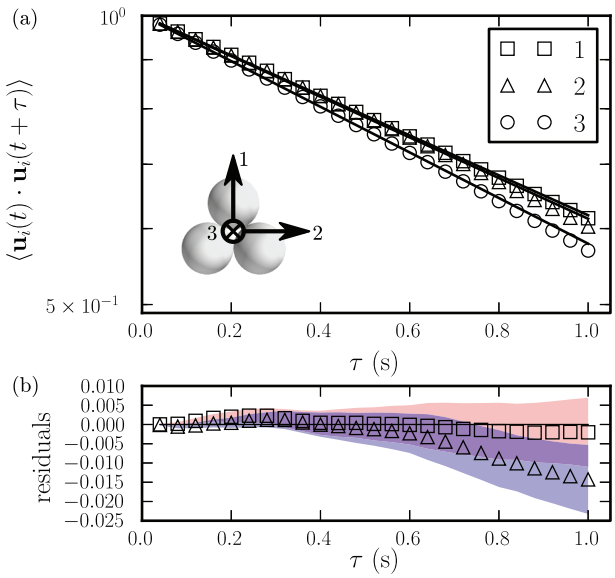

FIG. 3. (Color online) (a) Cluster axis autocorrelations $\langle \mathbf{u}_i(t) \cdot \mathbf{u}_i(t+\tau) \rangle$ for a trimer of 1-μm-diam spheres, showing anisotropic rotational diffusion. Open symbols are experimental measurements; error bars are comparable to or smaller than symbols. Solid lines are fits to exponential decays. The inset shows the cluster axis orientation. (b) Residuals for fits of a single exponential decay to the in-plane axis autocorrelations ($i = 1$ and 2). The solid line indicates the best-fit exponential. Red (light) and blue (dark) shaded regions denote error bars.

$a_{\text{eff}} = 709$ nm, which is larger than the optical radius $a_{\text{opt}} = 650$ nm obtained by fitting the holographic data. The larger effective radius is consistent with typical dynamic light scattering measurements of the size of colloidal spheres, which show enhanced hydrodynamic radii due to charge or hairy surface layers on the particles [33,34]. The best-fit viscosity is $\eta_{\text{eff}} = 1.159$ mPa s, consistent with measurements of the diffusion constant of a freely diffusing sphere in the same sample, which acts as an *in situ* thermometer, combined with bulk viscosity measurements using a Cannon-Manning capillary viscometer; these together give a solvent viscosity of 1.19 ± 0.04 mPa s. We use this procedure because the solvent viscosity has a strong temperature dependence [27]. The elements of $\mathbf{D}$ computed with these effective parameters agree with our measurements to better than 1% (Table I). We also note that the HYDROSUB prediction for $D_{r,\perp}$ differs from the analytical prediction by about 1%, which is consistent with prior studies [4]. The agreement between our measurements and the analytical prediction suggests that our measurement accuracy is at least comparable to, if not better than, that of HYDROSUB.

TABLE I. Measured diffusion tensor elements for the dimer in Fig. 2, along with analytical calculations from an exact Stokes solution [3] and numerical calculations from HYDROSUB [31]. Calculations use a best-fit particle radius $a_{\text{eff}} = 709$ nm and solvent viscosity $\eta_{\text{eff}} = 1.159$ mPa s. Experimental uncertainties are determined from best fits in Fig. 2; see [27] for details.

	Experiment	Exact	HYDROSUB
$D_{r,\perp}$ (s^{-1})	0.1034 ± 0.0006	0.1034	0.104
$D_{\parallel}$ ($\times 10^{-13}$ m^2 s^{-1})	2.015 ± 0.012	2.010	2.02
$D_{\perp}$ ($\times 10^{-13}$ m^2 s^{-1})	1.785 ± 0.007	1.790	1.80
$D_{\parallel}/D_{\perp}$	1.129 ± 0.011	1.123	1.12

Measurements on trimers reveal anisotropic translational and rotational diffusion. Trimers of identical particles have two mirror planes, making $\mathbf{D}^{tt}$ and $\mathbf{D}^{rr}$ diagonal [22,35] in the coordinate system shown in the inset of Fig. 1(b). We denote the six diagonal elements by $D_{t,1}$, $D_{t,2}$, $D_{t,3}$, $D_{r,1}$, $D_{r,2}$, and $D_{r,3}$. In contrast to dimers, trimers lack axisymmetry, allowing us to observe rotations about all three axes and measure all six elements. In Fig. 3(a), we show the axis autocorrelations $\langle \mathbf{u}_i(t) \cdot \mathbf{u}_i(t+\tau) \rangle$ computed from 20 000 hologrames, as well as best fits to exponential decays. The autocorrelation of axis 3 decays more rapidly than the autocorrelations of axes 1 and 2, in agreement with expectations: As shown in Eq. (3), $\langle \mathbf{u}_3(t) \cdot \mathbf{u}_3(t+\tau) \rangle$ depends on $D_{r,1}$ and $D_{r,2}$, both of which should be larger than $D_{r,3}$ due to hydrodynamics. The elements of the diffusion tensor that we extract from these data are shown in Table II. The difference between $D_{r,3}$ and both $D_{r,1}$ and $D_{r,2}$ is much larger than the experimental uncertainty, showing clear evidence for anisotropic rotational diffusion. The translational diffusion we observe is similarly anisotropic (Fig. 4 and Table II).

Interestingly, although our measurements of the dimensionless ratios $D_{r,1}/D_{r,3}$ and $D_{t,1}/D_{t,3}$ agree well with the HYDROSUB predictions, we observe small but statistically significant differences between the elements of $\mathbf{D}$ corresponding to the two in-plane axes 1 and 2. Figure 3(b) indicates that the autocorrelations of axes 1 and 2 are poorly fit by a single exponential decay. If the particles in the trimer are identical, the threefold symmetry axis of the trimer ensures that $D_{t,1} = D_{t,2}$

TABLE II. Measured diffusion tensor elements for trimer shown in Figs. 3 and 4 with comparisons to computations from HYDROSUB [31]. Computations use $a = 500$ nm obtained optically from the best-fit hologram models and $\eta = 1.049$ mPa s from single-particle diffusion data; the difference in η from the dimer measurements is due to a difference in room temperature. Experimental uncertainties determined from best fits in Figs. 3 and 4; see [27] for details.

	Experiment	HYDROSUB
$D_{r,1}$ (s^{-1})	0.278 ± 0.002	0.296
$D_{r,2}$ (s^{-1})	0.270 ± 0.002	0.296
$D_{r,3}$ (s^{-1})	0.210 ± 0.002	0.220
$D_{r,1}/D_{r,3}$	1.32 ± 0.02	1.34
$D_{r,1}/D_{r,2}$	1.03 ± 0.02	1.00
$D_{t,1}$ ($\times 10^{-13}$ m^2 s^{-1})	2.466 ± 0.015	2.64
$D_{t,2}$ ($\times 10^{-13}$ m^2 s^{-1})	2.446 ± 0.015	2.64
$D_{t,3}$ ($\times 10^{-13}$ m^2 s^{-1})	2.372 ± 0.015	2.41
$D_{t,1}/D_{t,3}$	1.04 ± 0.01	1.09

and $D_{r,1} = D_{r,2}$.[2] Thus the differences between these elements of the tensor imply that the particles in our trimer are not in fact identical. We performed HYDROSUB calculations to confirm that weakly breaking threefold symmetry results in differences between the in-plane elements of $\mathbf{D}$. Our measured ratio $D_{r,1}/D_{r,2} = 1.03 \pm 0.02$ corresponds to a 3% size difference between the spheres. This is consistent both with the particle manufacturer's certificate of analysis as well as with particle size differences determined from holograms. This shows that even a small amount of particle polydispersity can break the threefold rotational symmetry to a measurable degree.

Overall, our work demonstrates experimentally how both large and small differences in the symmetry of small particles affect the diffusion tensor. The technique we use, holographic microscopy, can measure elements of the diffusion tensor to high precision, 1% or better, small enough to resolve weak symmetry breaking due to particle polydispersity. The high precision is enabled by the inherently short acquisition times of the technique, allowing us to study rapidly diffusing systems that we can image for up to hundreds of rotational diffusion times $1/D_{r,i}$. These longer time scales more clearly reveal anisotropy in the diffusion tensor. Although here we have measured the diffusion of isolated clusters, it should be possible to use the same technique to measure diffusion tensors in environments that are relevant to self-assembly but challenging for computation. In particular, it may be possible to measure diffusion tensors near boundaries or other particles or for clusters that have internal degrees of freedom. The few studies examining the effect of interparticle hydrodynamic couplings on particle diffusion have been restricted to spheres in planar geometries [36–38]. Furthermore, measurements on other even less symmetric clusters may be able to reveal translational-rotational coupling as well as the off-diagonal rotational and translational elements in the diffusion tensor.

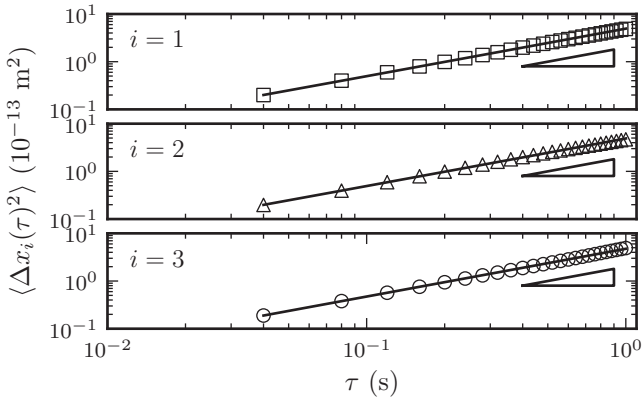

FIG. 4. Body-frame MSDs for the same trimer in Fig. 3. See the inset in Fig. 3(a) for axis orientations i. Open symbols are experimental measurements; error bars are comparable to or smaller than symbols. Solid lines are linear fits. Triangles show a MSD slope of 1.

We thank José García de la Torre, Daniela J. Kraft, Thomas G. Dimiduk, and Rebecca W. Perry for helpful discussions. This work was supported by the National Science Foundation through CAREER Grant No. CBET-0747625 and through the Harvard MRSEC, Grant No. DMR-0820484. We also acknowledge support from the Kavli Institute for Bionano Science & Technology at Harvard and an Alfred P. Sloan Research Fellowship.

[2] See [22,35]. Brenner does not explicitly treat discrete rotational symmetry, but his symmetry arguments are readily applied to this case.

[1] M. Holmes-Cerfon, S. J. Gortler, and M. P. Brenner, Proc. Natl. Acad. Sci. USA **110**, E5 (2013).
[2] F. Perrin, J. Phys. Radium **5**, 497 (1934).
[3] A. Nir and A. Acrivos, J. Fluid Mech. **59**, 209 (1973).
[4] J. García de la Torre, G. del Rio Echenique, and A. Ortega, J. Phys. Chem. B **111**, 955 (2007).
[5] P. Pakdel and S. Kim, J. Rheol. **35**, 797 (1991).
[6] S. A. Allison, Macromolecules **32**, 5304 (1999).
[7] S. Aragon and D. K. Hahn, Biophys. J. **91**, 1591 (2006).
[8] M. Hoffmann, C. S. Wagner, L. Harnau, and A. Wittemann, ACS Nano **3**, 3326 (2009).
[9] Y. Han, A. M. Alsayed, M. Nobili, J. Zhang, T. C. Lubensky, and A. G. Yodh, Science **314**, 626 (2006).
[10] Y. Han, A. Alsayed, M. Nobili, and A. G. Yodh, Phys. Rev. E **80**, 011403 (2009).
[11] S. M. Anthony, M. Kim, and S. Granick, J. Chem. Phys. **129**, 244701 (2008).
[12] M. Speidel, A. Jonás, and E.-L. Florin, Opt. Lett. **28**, 69 (2003).
[13] Z. Zhang and C.-H. Menq, Appl. Opt. **47**, 2361 (2008).
[14] R. Colin, M. Yan, L. Chevry, J.-F. Berret, and B. Abou, Europhys. Lett. **97**, 30008 (2012).

[15] D. Mukhija and M. J. Solomon, J. Colloid Interface Sci. **314**, 98 (2007).
[16] G. L. Hunter, K. V. Edmond, M. T. Elsesser, and E. R. Weeks, Opt. Express **19**, 17189 (2011).
[17] R. W. Perry, G. Meng, T. G. Dimiduk, J. Fung, and V. N. Manoharan, Faraday Discuss. **159**, 211 (2012).
[18] S.-H. Lee, Y. Roichman, G.-R. Yi, S.-H. Kim, S.-M. Yang, A. van Blaaderen, P. van Oostrum, and D. G. Grier, Opt. Express **15**, 18275 (2007).
[19] J. Fung, K. E. Martin, R. W. Perry, D. M. Kaz, R. McGorty, and V. N. Manoharan, Opt. Express **19**, 8051 (2011).
[20] J. Fung, R. W. Perry, T. G. Dimiduk, and V. N. Manoharan, J. Quant. Spectrosc. Radiat. Transfer **113**, 2482 (2012).
[21] T. M. Kreis, Opt. Eng. **41**, 1829 (2002).
[22] H. Brenner, J. Colloid Interface Sci. **23**, 407 (1967).
[23] S. Harvey and J. García de la Torre, Macromolecules **13**, 960 (1980).
[24] A. M. Yake, R. A. Panella, C. E. Snyder, and D. Velegol, Langmuir **22**, 9135 (2006).
[25] L. P. Faucheux and A. J. Libchaber, Phys. Rev. E **49**, 5158 (1994).
[26] D. W. Mackowski and M. I. Mishchenko, J. Opt. Soc. Am. A **13**, 2266 (1996).
[27] See Supplemental Material at http://link.aps.org/supplemental/10.1103/PhysRevE.88.020302 for further details on experimental methods and data analysis.
[28] L. D. Favro, Phys. Rev. **119**, 53 (1960).
[29] M. Doi and S. F. Edwards, *The Theory of Polymer Dynamics* (Clarendon, Oxford, 1986).
[30] F. C. Cheong and D. G. Grier, Opt. Express **18**, 6555 (2010).
[31] J. García de la Torre and B. Carrasco, Biopolymers **63**, 163 (2002).
[32] H. Flyvbjerg and H. G. Petersen, J. Chem. Phys. **91**, 461 (1989).
[33] J. E. Seebergh and J. C. Berg, Colloids Surf. A **100**, 139 (1995).
[34] M. R. Gittings and D. A. Saville, Colloids Surf. A **141**, 111 (1998).
[35] J. R. Happel and H. Brenner, *Low Reynolds Number Hydrodynamics* (Kluwer, Dordrecht, 1991).
[36] J. C. Crocker, J. Chem. Phys. **106**, 2837 (1997).
[37] J. W. Merrill, S. K. Sainis, J. Bławzdziewicz, and E. R. Dufresne, Soft Matter **6**, 2187 (2010).
[38] P. P. Lele, J. W. Swan, J. F. Brady, N. J. Wagner, and E. M. Furst, Soft Matter **7**, 6844 (2011).